Tomas Bata University in Zlín
Library

Hierarchically porous surface of PEEK/nMCS composite created by femtosecond laser and incorporation of resveratrol exhibiting antibacterial performances and osteogenic activity in vitro

Citation

CAI, Guiquan, Hui WANG, Yun Kyung JUNG, Zhiyan XU, Jiahong ZHANG, Jiye HE, Dongliang WANG, Jung-Woog SHIN, Rames KAEWMANEE, Jie WEI, and Nabanita SAHA. Hierarchically porous surface of PEEK/nMCS composite created by femtosecond laser and incorporation of resveratrol exhibiting antibacterial performances and osteogenic activity in vitro. *Composites Part B: Engineering* [online]. vol. 186, Elsevier, 2020, [cit. 2023-02-02]. ISSN 1359-8368. Available at https://www.sciencedirect.com/science/article/pii/S1359836819360147

DOI

https://doi.org/10.1016/j.compositesb.2020.107802

Permanent link

https://publikace.k.utb.cz/handle/10563/1009576

This document is the Accepted Manuscipt version of the article that can be shared via institutional repository.

TBU Publications
Repository of TBU Publications
publikace.k.utb.cz

Hierarchically porous surface of PEEK/nMCS composite created by femtosecond laser and incorporation of resveratrol exhibiting antibacterial performances and osteogenic activity in vitro

Guiquan Cai[a,1] , Hui Wang[a,1] , Yun Kyung Jung[b] , Zhiyan Xu[c] , Jiahong Zhang[a] , Jiye He [a,] , Dongliang Wang[a,*] Jung-Woog Shin[b], Rames Kaewmanee[c], Saha Nabanita[d], Jie Wei[c]**

[a]*Department of Orthopedic Surgery, Xin-Hua Hospital, Shanghai Jiao-Tong University School of Medicine, 1665 Kongjiang Road, Shanghai, 200092, China*

[b]*School of Biomedical Engineering, Inje University, Inje-ro 197, Gimhae, Gyeongnam, 50834, South Korea*

[c]*Key Laboratory for Ultrafine Materials of Ministry of Education, East China University of Science and Technology, Shanghai, 200237, China*

[d]*Centre of Polymer Systems, University Institute, Tomas Bata University in Zlin, Tr T Bati 5678, Zlin, 76001, Czech Republic*

[*] *Corresponding author.*

[**] *Corresponding author.*

E-mail addresses: hejiye@xinhuamed.com.cn (J. He), wangdongliang@xinhuamed.com.cn (D. Wang).
[1] *Guiquan Cai and Hui Wang contribute equally to this work.*

ABSTRACT

To further improve the surface properties of polyetheretherketone (PEEK)/nanoporous magnesium calcium silicate (nMCS) composite (PMC), hierarchically porous surface of PMC (PMCF) were created by femtosecond laser, and resveratrol (RV) was incorporated into the porous surface of PMCF (RV@PMCF). Compared to PMC with flat surface, PMCF contained not only two types of micropores with different sizes (around 20 pm and 0.5 pm) but also nanopores (around 4 nm), which exhibited remarkably increase in surface roughness and protein adsorption. In addition, PMCF displayed a slow-release of RV while PMC showed a burst-release of RV into cell cultured medium. Moreover, compared with PMC and PMCF, RV@PMCF with antibacterial performances inhibited the growth of E. coli and S. aureus thanks to the release of RV. In addition, compared with PMC, PMCF and RV@PMCF significantly promoted adhesion and proliferation of rat bone mesenchymal stem cells (BMSC). Furthermore, compared with PMCF, RV@PMCF obviously enhanced the proliferation and osteogenic differentiation as well as bone related genes expressions of BMSC. The results demonstrated that PMCF with hierarchically porous surface and incorporating of RV displayed antibacterial performances and osteogenic activity *in vitro*, Therefore, as a drug-loaded implant, RV@PMCF with good cytocompatibility would have a big potential for applications in orthopaedic fields.

Keywords: Polyetheretherketone based composite Femtosecond laser Hierarchically porous surface Antibacterial performances Osteogenic activity

1. Introduction

In the last few decades, polyetheretherketone (PEEK) has been widely studied and applied in spinal fusion, trauma and cranio-maxillofacial procedures, dental and joint replacements because of its excellent biocompatibility, outstanding mechanical performances and biological stability as well as radiolucency and so on **[1,2]**. Nowadays, PEEK has gradually become a popular implantable biomaterial in the fields of dental and orthopedics **[2]**. However, as a bioinert material, PEEK implant displays no osteogenic activity, which does not have the capability to promoting new bone tissue formation and osseointegration to achieve an initial fixation as well as long-term bio-stability **[3,4].**

Therefore, for orthopedic applications, enhancement of the osteogenic activity of PEEK has become one of the great challenges. More studies have been conducted to improve the osteogenic activity of PEEK, such as surface modification (physical or chemical methods), composites with bioactive fillers, and so on **[5-7]**. However, it is difficult for single treatments by physical or chemical ways to significantly improve the osteogenic activity of PEEK **[5-7]**. Moreover, PEEK based composites were generally fabricated by addition of fillers (e.g., bioactive glass-es/ceramics) into PEEK matrix with appropriate content **[8,9]**. Although the composites containing bioactive fillers exhibited some improved mechanical properties and osteogenic activity, most of the fillers were dispersed into PEEK matrix, which did not significantly improve the surface osteogenic activity because only a few bioactive fillers were exposed on the composite surface **[8,9]**. Surface properties (e.g., composition, topography, roundness, porous structure) of the implantable biomaterials have critical effects on cells behaviours and functions both *in vitro* and *in vivo* **[10]**. Therefore, it is quite necessary to modify the surface of PEEK based composites to further improve the surface properties, especially, osteogenic activity.

In recent years, femtosecond laser (FL) technology has been utilized to improve the surface performances of various materials (e.g., metal, polymer and inorganic material). FL is capable of forming a uniform, regular three-dimensional structure on material surface, and the surface-modified layer is thin that has little effect on the properties of substrate material **[11]**. In addition, FL is an effective technology to fabricate periodical features with micrometer- or nanometer-scale topography on the surface of substrate **[12]**. The advantages of FL include the simplicity in varying processing conditions, rapid scanning speed, high dimensional accuracy and high reproducibility as well as minimal oxidation of materials surfaces during processing **[13,14]**. More importantly, the application of FL to perforate the biomaterial surface can form a uniform array of pits, which can not only stimulate the ingrowth of bone tissue but also be incorporated with drugs that enhance osteogenic and antibacterial properties, to promote new bone formation and osseointegra-tion **[15]**. Furthermore, it is widely applied to directly incorporate the drugs into the porous surface of the implant, which can directly act on the wound that improves the speed of bone healing.

The surface of implantable biomaterial during the operation is prone to adhesion of bacteria and formation of biofilm, leading to biomaterial-related infections, which ultimately causes the failure of implants **[16]**.

Peri-operative and latent infections have become the major reasons for spinal, hip and knee revision surgery **[17]**. Infections are devastating for the patients, which require removal of the implanted medical device, followed by re-implanting of a new implant **[17]**. Therefore, research and development of implantable biomaterials with anti-infection has attracted considerable attention in orthopaedic application. Resveratrol (RV) is a polyphenolic phytoestrogen present in some plants (e.g., berries, peanuts and grapes), which not only possesses outstanding antibacterial performances but also has osteogenic activity **[18]**. RV had strong antibacterial effects on methicillin-resistant *Staphylococcus aureus* by the minimum inhibitory concentration of RV against various bacteria **[19]**. RV has been

demonstrated to significantly improve the symptoms of bone loss in ovariectomized rats **[20]**. Studies have shown that RV enhanced the proliferation as well as differentiation of osteoblasts, and stimulated new bone regeneration by regulating bone-related signals **[21]**. RV can improve the activity of the ERK pathway while inhibit the activity of GSK-3β, and promote the stability of p-catenin and activate the signaling pathway of Wnt/β-catenin, thereby promoting osteogenic differentiation of the osteoblasts **[21,22]**.

Nanoporous bioactive glass with large surface area as well as high porosity has been proved to possess high bioactivity, stimulate osteoblasts responses and quickly improve new bone formation compared with traditional bioactive glass **[23]**. In our previous study, PEEK based bioactive composite containing nanoporous magnesium calcium silicate (nMCS) has been prepared, and the PEEK/nMCS composite (PMC) containing 40w% nMCS exhibited higher mechanical properties and better bioactivity than PEEK alone **[24,25]**. To further improve the surface properties of PMC as an implantable material for orthopedic applications, hierarchically porous surface of PMC (PMCF) was created by FL, and RV was incorporated into the porous surface of PMCF (RV@PMCF) in this study. We assume that RV@PMCF with hierarchically porous surface and incorporating of RV possess not only antibacterial performances but also osteogenic activity. To confirm the hypothesis, the surface properties (e.g., porous morphology, roughness and protein adsorption as well as ions release), antibacterial performances and cellular responses of bone mesenchymal stem cells (BMSC) of rat to RV@PMCF were investigated.

2. Materials and methods

2.1. Fabrication and characterization of specimens

Nanoporous magnesium calcium silicate (nMCS) was prepared using a sol-gel method **[25]**. Briefly, 13.2 g cetyltrimethylammonium bromide was dissolved into water (1000 mL), and 25 mL ammonia aqueous solution (28 w%) was subsequently added into the solution with continuous stirring for 60 min. Subsequently, 55.8 g tetraethyl orthosilicate (98%), 34.4 g magnesium nitrate hexahydrate and 31.6 g calcium nitrate tetrahydrate were also dissolved into this solution, and stirred for 4 h. The products were filtered and rinsed with deionized water as well as absolute ethanol (3 times), which then was dried at 90 °C and sintered at 600 °C for 5 h to get the nMCS powders. Transmission electron microscopy (JEM-2010, JEOL Ltd, Japan) as well as Brunauer-Emmett-Teller (Tristar 3000, Micromeritics, USA) were used to characterized the nMCS powders.

Polyetheretherketone (PEEK)/nMCS composite (PMC) containing 40w% nMCS was fabricated by a way of cold pressing-sintering. PEEK powder (Victrex, UK) and nMCS powder were mixed using planetary ball mill (QM-3SP2, Nanda Instrument Co., China) in the predetermined ratio. Then, the mixed powder was put into stainless-steel mold (ϕ12 x 2 mm), and then pressed using pressure machine (YP-40T, Jinfulun Co., China) with the pressure (4 MPa) for 2 min. The obtained specimens were placed in a furnace (SX2-8-10 N, Yiheng Co., China), and sintered at 350 °C (heating rate: 2 °C/min) for 2 h. The surfaces of specimens (PMC) were polished and washed sequentially with ethanol and deionized water. The samples surfaces were further treated by an instrument of femtosecond laser (FL,GLX-200HP-1053, Time-Bandwidth Products AG Co., Switzerland). In brief, the samples were placed on a programmed two-dimensional mobile platform with perforation power of 20 mW, pulse width of <200 fs and center wavelength of 800 nm as well as repetition rate of 1 kHz. The samples (PMCF) treated by FL were then sonicated with deionized water and subsequently ethanol for further use.

The samples (PMC and PMCF) were immersed into PBS solution containing 0.5 mg/mL resveratrol (RV, Sigma-Aldrich Co., USA), and placed into a constant temperature oscillator (HZQ-X300, Yiheng Co.,

China) at 37 ° C for 24 h. Moreover, the samples were taken out and washed by using ethanol (100 mL) to remove the unloaded RV. Finally, the samples were dried in air (at 37 °C) for 24 h to obtain RV-loaded PMC (RV@PMC) and PMCF (RV@PMCF).

Both PMC and PMCF were immersed into PBS solution containing 0.5 mg/mL resveratrol (RV, Sigma-Aldrich Co., USA), and placed into a constant temperature oscillator (HZQ-X300), which was purchased from Yiheng Co., China at 37 °C for 24 h. Moreover, the specimens were taken out and washed by 100 mL ethanol to remove the unloaded RV. Finally, the specimens were dried in air (at 37 °C) for 24 h to obtain RV-loaded PMC (RV@PMC) and PMCF (RV@PMCF). The samples (nMCS, RV, PMCF and RV@PMCF) were analyzed by Fourier transform infrared spectroscopy (Nicolet 5700) from Nicolet Co., USA as well as X-ray diffractometer (Rigaku D/max 2550, Japan). Furthermore, scanning electron microscope (S-3400 N, Hitachi Co., Japan) as well as laser confocal 3D microscope (VK-X110, Keyence Co., Japan) were applied to characterize the surfaces of PMC, PMCF and RV@PMCF.

2.2. Protein adsorption and RV load/release from specimens

Protein adsorption (bovine serum albumin, BSA) on the surface of the samples (PMC, PMCF and RV@PMCF) was determined by |iBCA kit. Briefly, the samples were placed into 24-well plate, and BSA solution (10 μg/mL) was added into the plate. After incubation at 37 °C for 4 h under static conditions, the samples were removed and rinsed using PBS for 3 times to remove the un-adsorbed protein. The samples were then placed into 5% sodium dodecyl sulfate and shaken (at 37 °C) to release the adsorbed protein. Finally, the solution was collected and the adsorbed protein was quantified by using μBCA assay. The results were expressed as the mass of bovine serum albumin (protein/sample, mg/g) which was adsorbed per unit mass of sample.

The release of RV from the sample was detected by immersing RV@PMC and RV@PMCF into the cell cultured medium for different time. The specimen was immersed into the medium (50 mL for each specimen), which were placed into a constant temperature oscillator. At different time points, 1 mL culture broth was taken, followed by adding of 1 mL fresh medium. The absorbance of RV onto the samples was measured (at a wavelength of 306 nm) utilizing a microplate reader. The cumulative release (CR) was calculated by using the formula of CR = (C x V)/W, where C was RV concentration (at different time), V was solution volume, and W was totally loading amount of RV onto the samples.

2.3. Antibacterial performances

Escherichia coli (E. coli) as *well as Staphylococcus aureus (S. aureus)* was utilized as bacterial models. The samples (PMC, PMCF and RV@PMCF) were cultured with bacteria for 24 h and the percentage of bacterial reduction was measured by colony counting. The specific operation steps of the antibacterial experiment were shown as follows: both *E. coli* and *S. aureus* liquids of 105 CFU/mL were prepared, and 20 mL of the bacterial liquid was placed into centrifuge tube together with the samples, and placed into constant temperature oscillator at 37 °C with the oscillating frequency of 250 r/min, so that the samples and bacterial liquid were fully contact. At 24 h after culturing, 0.1 mL broth of E. coli and *S. aureus* was taken out from the bottle, and dropped on a pre-sterilized and cooled agar medium. It was then coated with a sterile-cooled glass rod to spread the bacterial solution evenly over the agar medium. Each plate was placed upside down in an incubator until *E. coli* and *S. aureus* grew onto the medium. After 24 h, the plate medium was taken out, then the *E. coli* colonies as well as *S. aureus* colonies were counted. The percent reduction of bacteria was calculated as following: Percent

reduction of bacteria = (N-M)/N x 100%, where M was the number of colonies in the experimental group and N was the number of colonies in the blank control group.

2.4. Cells responses to samples

Bone mesenchymal stem cells (BMSC) were extracted from the rat limbs bone marrow. SD rats were sacrificed by cervical dislocation, and immersed in 75% medical alcohol for 10 min, and the serum-free medium was pumped through a syringe to wash the marrow cavity until it turned white. The cells were centrifuged at a speed of 8000 rpm, and after removing the supernatant, the Minimum Essential Medium (Thermo Fisher Scientific, USA) was added supplemented with fetal bovine serum (10%, Hyclone, Australia) and penicillin/streptomycin (1%, Sigma, China), and the cell culture procedure was carried in a humidified 5% CO_2 incubator (37 °C). The medium was replaced every two days. Experiments were performed using passage 3 rat mesenchymal stem cells. The cells were digested with trypsin (0.25%) and detached, and cell suspensions were formed, and the cell suspension was counted before culturing on the samples (PMC, PMCF and RV@PMCF). The seeding density of the cells was 1 x 10^4 cells for each well (24-well plate), and every 2 days, the cell cultured medium was changed.

2.4.1. Cell attachment and morphology

The samples were sterile autoclaved, and then were cultured with the cells. After incubating for 12 h, 24 h, the samples were taken out, gently rinsed by using PBS solution (3 times), and fixed by using 0.25% glutaraldehyde solution. Then, dehydration was carried out stepwise by ethanol solution with the concentrations of 10%, 30%, 50%, 70%, 85%, 90% and 100% for 15 min. The cell morphology on the samples was observed utilizing scanning electron microscope. Cell Counting Kit-8 (Sigma-Aldrich, China) was utilized to determine the adhesion of the

BMSC on the specimens. At different time (6, 12 and 24 h) after culturing, the specimens were rinsed by using sterile PBS for 3 times, and the samples were sifted into another 24-well plate. A 400 μL cell medium containing Cell Counting Kit-8 solution (40 μL) was prepared. The working solution was put into the well plate, and incubated in an incubator for 6 h. After that, the supernatant was changed into a 96-well plate, and the optical density (OD) value was determined at 450 nm with a microplate reader (384 SpectraMax, Molecular Devices, USA).

2.4.2. Cell proliferation and ALP activity

Cell proliferation was evaluated after co-cultured with samples. The BMSC was seeded on the samples surfaces (density of 1 x 10^4 cells for each well) in a 24-well plate. Cell proliferation at different times (1, 3 and 7 days) was tested using a CCK-8 kit, and finally the OD value was obtained utilizing a microplate reader. ALP activity of the BMSC on the specimens was evaluated at 7, 10 and 14 days after culturing. The cells were seeded onto the samples and tissue culture plates were used as controls. At different time after cells culturing, the medium was discarded, and the specimens were washed by PBS (3 times). The 500 μL Nonidet P-40 (1%) solution was put into each well, and the cell lysate was obtained by lysing cells for 1 h to a. Then 50 μL of 1 mg/mL nitrophenyl phosphate disodium salt (p-nitrophenyl phosphate, Songon, China) solution, including glycine (0.1 mol/L) as well as magnesium chloride hexahydrate (1 mmol/L, pH = 9) was put into each well, which was incubated in an incubator at 37 °C for 1 h. Finally, 100 μL of 0.1 mol/L NaOH solution was put into each well to terminate the

color reaction. The OD values were measured at 405 nm by utilizing a microplate reader. The total protein contents in the lysate was determined by utilizing bovine serum albumin as a standard protein and assayed using a BCA kit (Biyuntian Biotechnology, China). The OD values/total protein contents at 405 nm was expressed as ALP activity.

2.4.3. Bone related gene expressions

The BMSC (density of 2 x 10^4 cells/well) were cultured on the specimens for 7 and 14 days, and the expression of bone related gene was detected utilizing real-time polymerase chain reaction (RT-PCR). By using a TRIzol reagent (Invitrogen, USA), the total RNA was extracted, and the total amount of RNA was tested by an ultraviolet spectrophotometer and reverse transcribed using a gene amplification instrument. Using the cDNA obtained by reverse transcription as a template, the expression of the relevant osteogenic gene was detected by a SYBR® Premix Ex TaqTM (Takara, Japan), and RT-PCR was performed utilizing a Bio-Rad real-time PCR system (Hercules, USA). Glyceraldehyde-3-phosphate dehydrogenase (GAPDH) was applied as housekeeping gene, and four bone related genes (osteopontin, osteocalcin, alkaline phosphatase, runt-associated transcription factor 2) were detected. **Table 1** listed the forward and reverse primers for the selected genes. For each gene, the relative expression level was calculated and normalized to glyceraldehyde-3-phosphate dehydrogenase.

2.5. Ions release from specimens into medium

After immersed into cell cultured medium for different time, the release of Si, Mg and Ca ions from the specimens was evaluated. At 1, 4, 7, 10 and 14 days, the medium was collected and centrifuged at 1500 rpm. The supernatant was mixed with HNO_3 solution (0.3 mol/L) at a volume ratio of 1/2 and the concentrations of Si, Mg and Ca ions in solution were evaluated by Inductivity Coupled Plasma (ICP-OES, Agilent IC, USA).

Table 1 Primer pairs used in real-time PCR analysis.

Gene	Forward primer (5′-3′)	Reverse primer (5′-3′)
Runx2	AACAGCAGCAGCAGCAGCAG	GCACGGAGCACAGCAAGTTGG
ALP	TGACCGTCCTGCTGGAACTCG	CCACTGCCACACTTGTCACACAG
OPN	GACGATGATGACGACGACGATGAC	GTGTGCTGGCAGTGAAGGACTC
OCN	AGACCTAGCAGAGACCATGAGGAC	TGAGGTAGCGCCGGAGTCTATTC
GAPDH	ACAGCAACAGGGTGGTGGAC	TTTGAGGGTGCAGCGAACTT

2.6. Statistical analysis

The data of experimental results were indicated as mean ± standard deviation for 3 samples. In addition, with Tukey's post hoc test, the results were analyzed by one-way ANOVA, and the significant difference was statistically considered ($p < 0.05$).

3. Results

3.1. Surface characteristics of samples

Form the TEM images (**Fig. 1**a) and pore diameter distribution (**Fig. 1**b) of the nMCS, it was seen that the nMCS displayed spherical morphologies with particles size of around 200 nm and nanopore size of around 4 nm. The fourier transform infrared spectroscopy (FTIR) of RV, PMCF, RV@PMCF and nMCS are displayed in **Fig. 1**c. For RV, the characteristic absorption at 965 cm^{-1} was trans carbon-carbon double bond (-C=C-) while at 1620 cm^{-1}, 1540 cm^{-1}, 1500 cm^{-1} were attributed to the benzene ring absorption peaks. For nMCS, the characteristic absorption of antisymmetric stretching vibration of siloxane bond (Si-O-Si) appeared at 1093 cm^{-1} as well as 799 cm^{-1}. As for PMCF, the characteristic bands of PEEK appeared, the peak at 1652 cm^{-1} was stretching vibration band of carbonyl (C═O), the peak at 1308 cm^{-1} was benzene in-plane vibration band of ether bond (R-O-R), the peak at 1226 cm^{-1} was stretching vibration band of R-O-R, the peak at 929 cm^{-1} was the stretching vibration of ketone bond (R-CO-R), the peak at 1163 cm^{-1} was in-plane bending vibration band of carbon-hydrogen bond (C-H), and the peaks at 840 cm^{-1} and 764 cm^{-1} were benzene out-plane bending vibration band. In addition, the characteristic peaks for nMCS and PEEK could be found in both PMC and PMCF. Furthermore, the peaks for PEEK, nMCS and RV could be observed in RV@PMCF. The X-ray diffractometer (XRD) patterns of RV, PMCF, RV@PMCF and nMCS are exhibited in **Fig. 1**d. The characteristic peaks of RV appeared at 2Θ = 13.20,16.3°,19.20,22.3° and 28.3°. For nMCS, a wide peak appeared at around 2Θ = 24°, indicating that nMCS was an amorphous phase. For PMC, PMCF and RV@PMCF, the peaks of PEEK at 2Θ = 18.7°, 20.8°, 22.8° and 28.8° were found while no obvious peak of nMCS appeared. Furthermore, the characteristic peaks of RV were not shown in RV@PMCF, suggesting that RV might be adsorbed into internal surface of micropores.

Fig. 1. TEM images (a) and pore diameter distribution (b) of the nMCS; FTIR (c) and XRD (d) of RV, PMCF, RV@PMCF and nMCS.

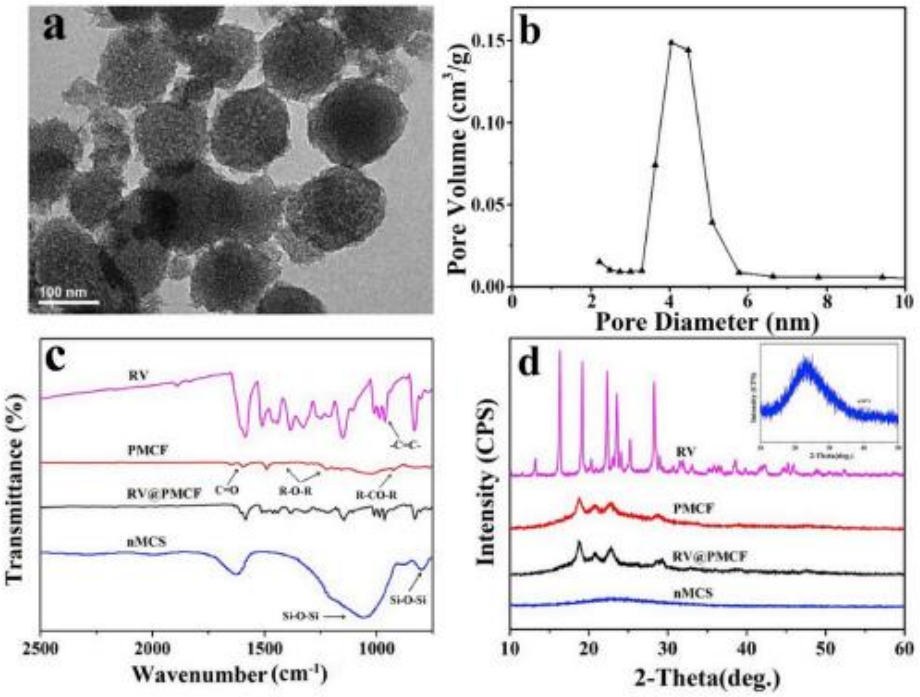

From the scanning electron microscope (SEM) photographs of the specimens, PMC displayed flat surface (**Fig. 2**a, low magnification) and many nMCS particles appeared on the surface (**Fig. 2**b, high magnification). After PMC was surface modified by femtosecond laser, many uniform micropores with the pore size of around 20 μm were created on PMCF surface (**Fig. 2**c, low magnification), and the internal surface of the micropore contained many submicro-pores (around 0.5 μm) (**Fig. 2**d, e, f, high magnification). Moreover, the RV was seen to be adsorbed onto the internal walls of the micropores **(Fig. 2**g and h). From the laser confocal microscope 3D photographs of the samples, it was found that PMC exhibited flat surface (**Fig. 3a**) while PMCF (**Fig. 3**b) and RV@PMCF (**Fig. 3**c) displayed mesh shaped surfaces with many uniform micropores. In addition, 2D profiles of the samples in the right bottom of the 3D photographs revealed that the diameter of micropores was around 20 μm and depth of micropores was around 30 μm. The surface roughness of the samples is displayed in **Fig. 3d**. As compared with PMC (Ra = 3.49 μm), the surface roughness of PMCF (Ra = 5.36 μm) significantly increased. However, no notable differences in surface roughness between PMCF and RV@PMCF (Ra = 5.64 μm) were seen.

3.2. Samples load/release of RV

The adsorption of RV onto surfaces of PMC and PMCF in the medium at different time is shown in **Fig. 4**a. At 48 h, the amount of RV onto PMCF was 9.8 mg/g while the amount of RV on PMC was 4 mg/g. The release of RV from RV@PMC and RV@PMCF at different time is shown in **Fig. 4**b. At the first day, cumulative releases of RV from RV@PMC and RV@PMCF were 70.2% and 15.4%. In addition, at the 20th day, cumulative releases of RV from RV@PMC and RV@PMCF were 70.2% and 80.4%. The results exhibited that RV@PMCF showed slow-release of RV into the medium while RV@PMC displayed a burst-release of RV.

3.3. Antibacterial performances of samples

From the photos (**Fig. 5**a) of E. coli as well as S. aureus colonies on the agar at 24 h after cultivating, many bacteria were found for both PMC and PMCF while no bacterium was seen for RV@PMCF. The percent reduction of E. coli for both PMC and PMCF was 0, for RV@PMCF was 97.8% (**Fig. 5**b). In addition, the percent reduction of S. aureus for both PMC and PMCF was 0, for RV@PMCF was 99.8% (**Fig. 5**c).

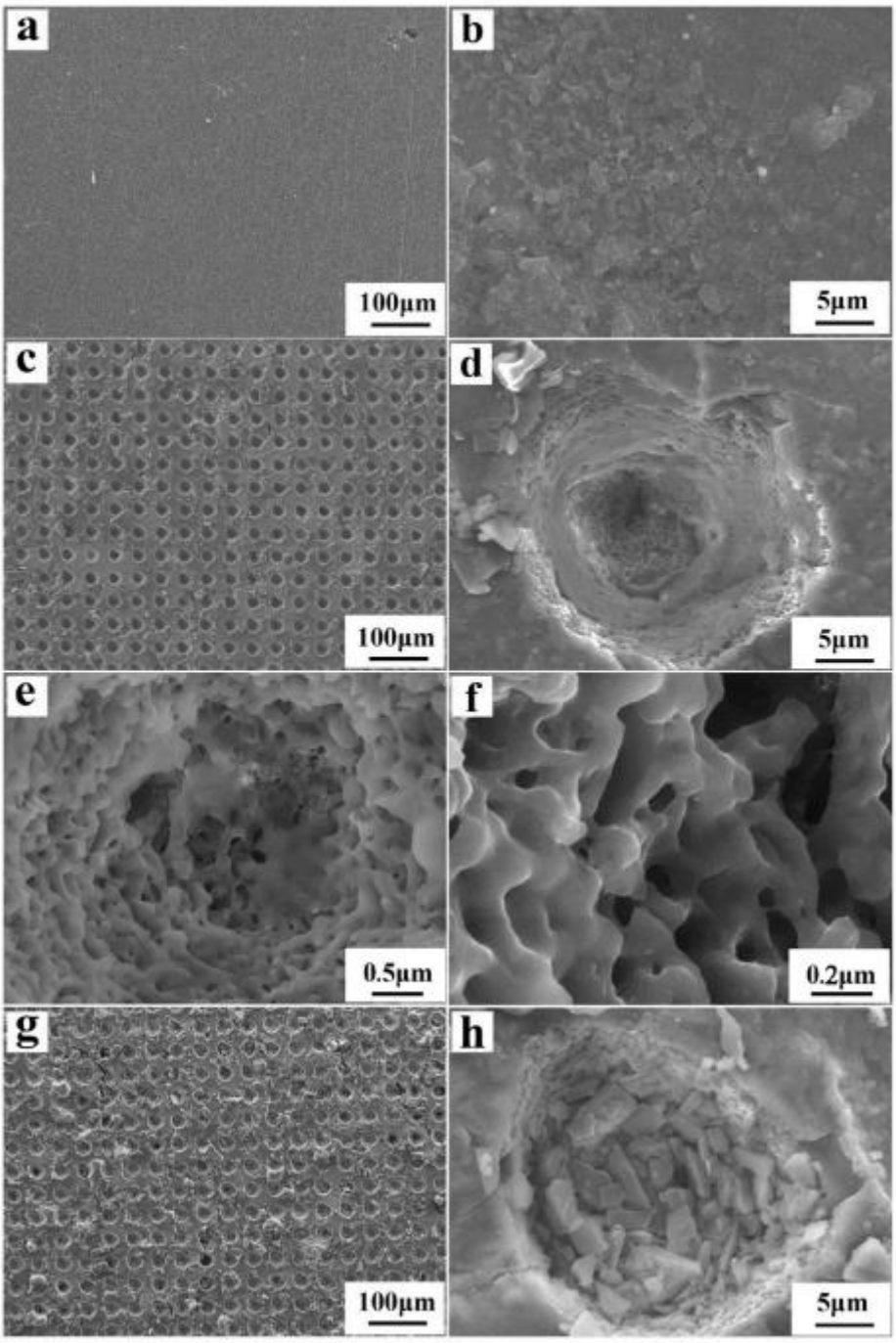

Fig. 2. SEM photographs of surface morphology of PMC (a, b), PMCF (c, d, e, f) and RV@PMCF (g, h) under low and high magnification.

3.4. Cells responses to samples

3.4.1. Protein adsorption, cell attachment and morphology

The adsorption amounts of bovine serum albumin (BSA) on PMC, PMCF and RV@PMCF were 0.8 ± 0.05, 1.3 ± 0.03 and 1.50 ± 0.06 mg/ g, which were show in **Fig. 6**a. The BMSC attachment ratio for the samples at different time after culturing is shown in **Fig. 6**b. At every point in time, the attachment ratio for PMCF and RV@PMCF were higher than those of PMC. At 24 h after culturing, the attachment ratio for PMCF (90.0 ± 3.5%) and RV@PMCF (92.4 ± 2.8%) were significantly higher than PMC (77.8 ± 4.1%).

The SEM micrographs of the BMSC on the samples (under different magnification) at 24 h after culturing are shown in **Fig. 6**c-h. The cells were seen to attach and spread on the sample surface, and the number of the attached cells on the sample for PMCF and RV@PMCF were remarkably higher than PMC. No remarkable differences for cell morphology as well as number of cells were seen between PMCF and RV@PMCF. In addition, the cells with expanded morphology and visible pseudopodia were seen to attach on the walls of micropores of both PMCF and RV@PMCF, which were seen to grow into the micropores (**Fig. 6e**-h).

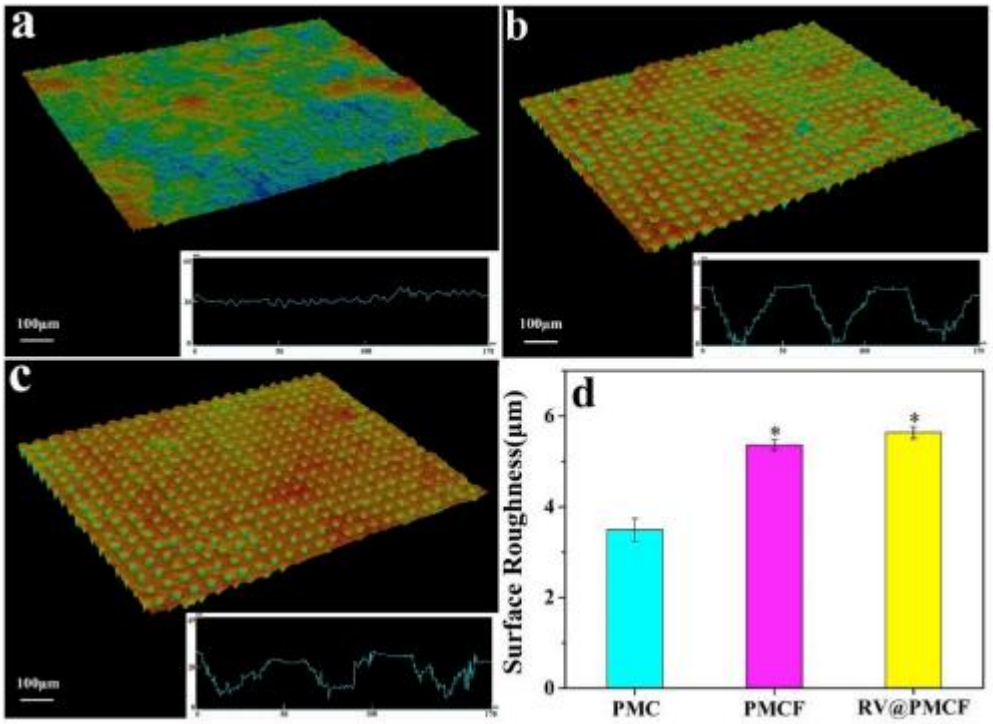

Fig. 3. Laser confocal microscope 3D photographs of PMC (a), PMCF (b) and RV@PMCF (c), and 2D profiles of the samples in the right bottom of the 3D photographs; surface roughness (d) of the samples (* represents $p<0.05$, vs PMC).

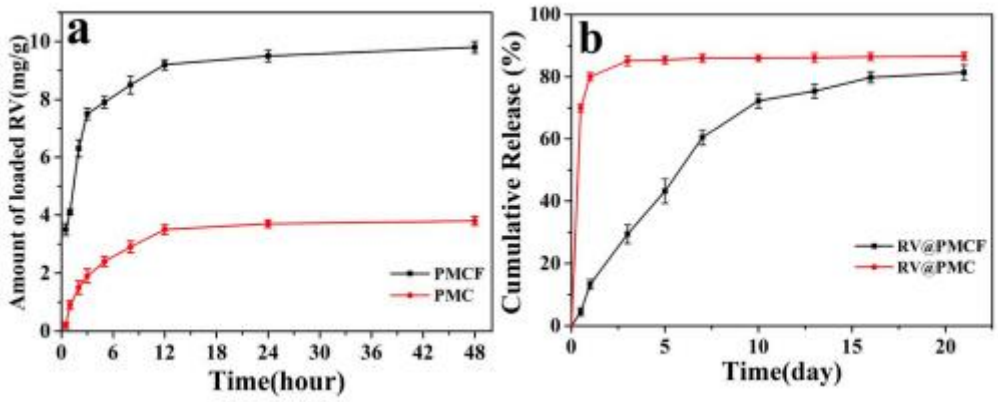

Fig. 4. Adsorption of RV (a) onto the surfaces of PMC and PMCF, and cumulative release of RV (b) from RV@PMC and RV@PMCF into medium at different time.

The CLSM photos of the cytoskeleton (stained by FITC) and nucleus (stained by DAPI) of BMSC cultured on the samples for 3 and 7 days were displayed in **Fig. 7.** The cells spread well on the samples surfaces, which exhibited a fusiform shape and extended the pseudopod. At 3 days, more cells attached onto the surfaces of PMCF and RV@PMCF than PMC. No notable differences of the cells number were seen between PMCF and RV@PMCF. At 7 days after culturing, more cells attached onto the surfaces of RV@PMCF than PMCF.

3.4.2. Ions release from specimens into medium

The alteration of ion concentration of Si, Mg and Ca in medium after the samples immersion for different time is exhibited in **Fig. 8.** These ions concentration for the samples increased with time. Furthermore, these ions concentrations for PMCF and RV@PMCF were higher than PMC during the soaking time. However, no significant difference in ion concentration between PMCF and RV@PMCF was seen, indicating that RV@PMCF loaded RV did not notably affect the release of these ions.

3.4.3. Cell proliferation and ALP activity

The OD values of BMSC on the samples at different time after culturing are displayed in **Fig. 9**a. At 1 day after culturing, the OD values for PMCF and RV@PMCF were notably higher than PMC while no notable differences were seen between PMCF and RV@PMCF. At 3 and 7 days after culturing, The OD value for RV@PMCF was the highest in all samples, and the OD value for PMCF was notably higher than PMC. The ALP activities of BMSC on the samples at different time after culturing are exhibited in **Fig. 9**b. At 7 days after culturing, no notable difference in ALP activity for PMC, PMCF and RV @ PMCF was seen. At 10 and 14 days, the ALP activity for RV@PMCF was notably higher than PMC and PMCF. No notable differences were seen in ALP activity between PMC and PMCF at 10 and 14 days after culturing.

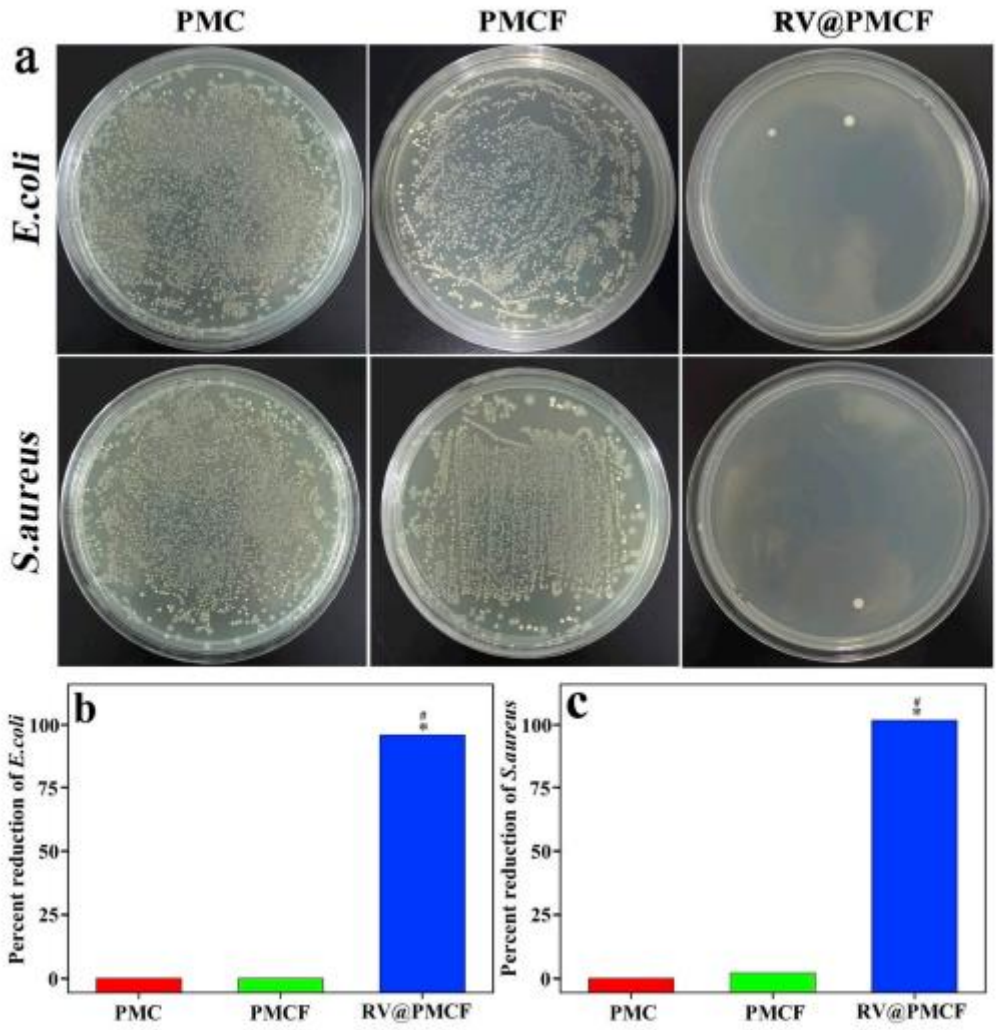

Fig. 5. Photos (a) of cultivated E. coli and S. aureus colonies on agar, which were dissociated from the samples, and percent reduction of E. coli (b) and S. aureus (c) for the samples (* represents $p<0.05$, vs PMC; # represents $p< 0.05$,vs PMCF).

3.4.4. Bone related gene expressions

The mRNA gene expression of runt-associated transcription factor 2 (Runx2), alkaline phosphatase (ALP) and osteopontin (OPN) as well as osteocalcin (OCN) are displayed in **Fig. 10**. At 7 days after culturing, the Runx2, ALP and OCN expressions for RV@PMCF were significantly higher than PMC and PMCF. Moreover, the OPN expression for RV@PMCF was remarkably higher than PMC and PMCF. Moreover, at 14 days after culturing, the Runx2, ALP and OCN expressions for RV@PMCF were significantly higher than those for PMC and PMCF. However, at both 7 and 14 days, no remarkable differences were seen for the expressions of Runx2, ALP, OPN and OCN between PMCF and PMC.

4. Discussions

Implantable biomaterials with antibacterial performances and osteogenic activity exhibit great potentials for orthopedic applications **[26].** As biomaterials for bone repair and substitute, surface characteristics (e. g., composition, porous morphology, roughness and ions release) have key

influences on cells behaviours and functions as well as osteogenic activity **[27-29]**. In this study, hierarchically porous structures on PEEK/nMCS composite (PMC) surface (PMCF) were created by femtosecond laser, and RV was incorporated into the porous surface of PMCF (RV@PMCF). Compared to PMC with flat surface, PMCF surface exhibited a uniform array of many micropores (sizes of around 20 μm), which contained many submicropores (sizes of around 0.5 μm) into the internal surface. Moreover, the internal surface of the micropores also included many nMCS with nanopores (sizes of around 4 μm) **[25]**. Therefore, PMCF surface contained not only two types of micropore with different sizes but also nanopores, indicating a hierarchically porous surface.

Surface roughness of the biomaterial has significant influences on cell adhesion, spreading, and subsequently cell proliferation, osteogenic differentiation and new bone regeneration **[30]**. In the present study, as compared with PMC, the surface roughness of PMCF and RV@PMCF significantly increased. Evidently, compared to PMC with flat surface, the hierarchically porous surface of PMCF obviously increased the surface area and porosity, and thus improved the loaded amount of RV (PMCF > PMC). However, no remarkable difference in surface roughness between PMCF and RV@PMCF was seen, suggesting that incorporating of RV into the porous surface had no obvious influences on the surface roughness. For the release of RV, the results showed that RV@PMCF exhibited a slow-release of RV while RV@PMC displayed a burst-release of RV. Therefore, the slow-release of RV was attributed to the porous surface of PMCF while the burst-release of RV was due to the flat surface of PMC.

The adhesion and growth of bacteria as well as formation of biofilms on the surface of biomaterials are the main causes of biomaterial-related infections, and the development of implantable biomaterials with antibacterial performances is likely to solve this serious problem **[31]**. Previous studies have shown that RV affected the growth and metabolism of bacteria by interfering with the synthesis of bacterial cell walls while damaging cell membranes, exhibiting antibacterial performances **[32]**. In the present study, RV@PMCF showed outstanding antibacterial properties against E. coli as well as S. aureus as compared with PMCF and PMC. Clearly, the antibacterial performances of RV@PMCF were ascribed to the release of RV.

Adsorption of proteins on biomaterial surface would promote the contact between cell membrane and materials surface, and improve the extension of pseudopodia, which would be favourable for cells adhesion **[33]**. In the present study, the adsorption of BSA on both PMCF and RV@PMCF were significantly higher than PMC. Therefore, compared with PMC, the enhancement of protein adsorption on both PMCF and RV@PMCF were ascribed to the presence of hierarchically porous surface, which increased surface area and porosity. Surface performances (e.g., porous morphology, roughness and protein adsorption) of the biomaterials play significant roles in cell behaviours and functions (e.g., adhesion and spreading) **[34]**. In the present study, the cell attachment as well as spreading on PMCF and RV@PMCF was much better than PMC. Moreover, compared with PMCF, incorporating of RV into RV@PMCF displayed no remarkable influences on cell adhesion as well as spreading. Therefore, the improvements of cell adhesion as well as spreading on PMCF and RV@PMCF were due to the presence of porous surface, which improved roughness and protein adsorption.

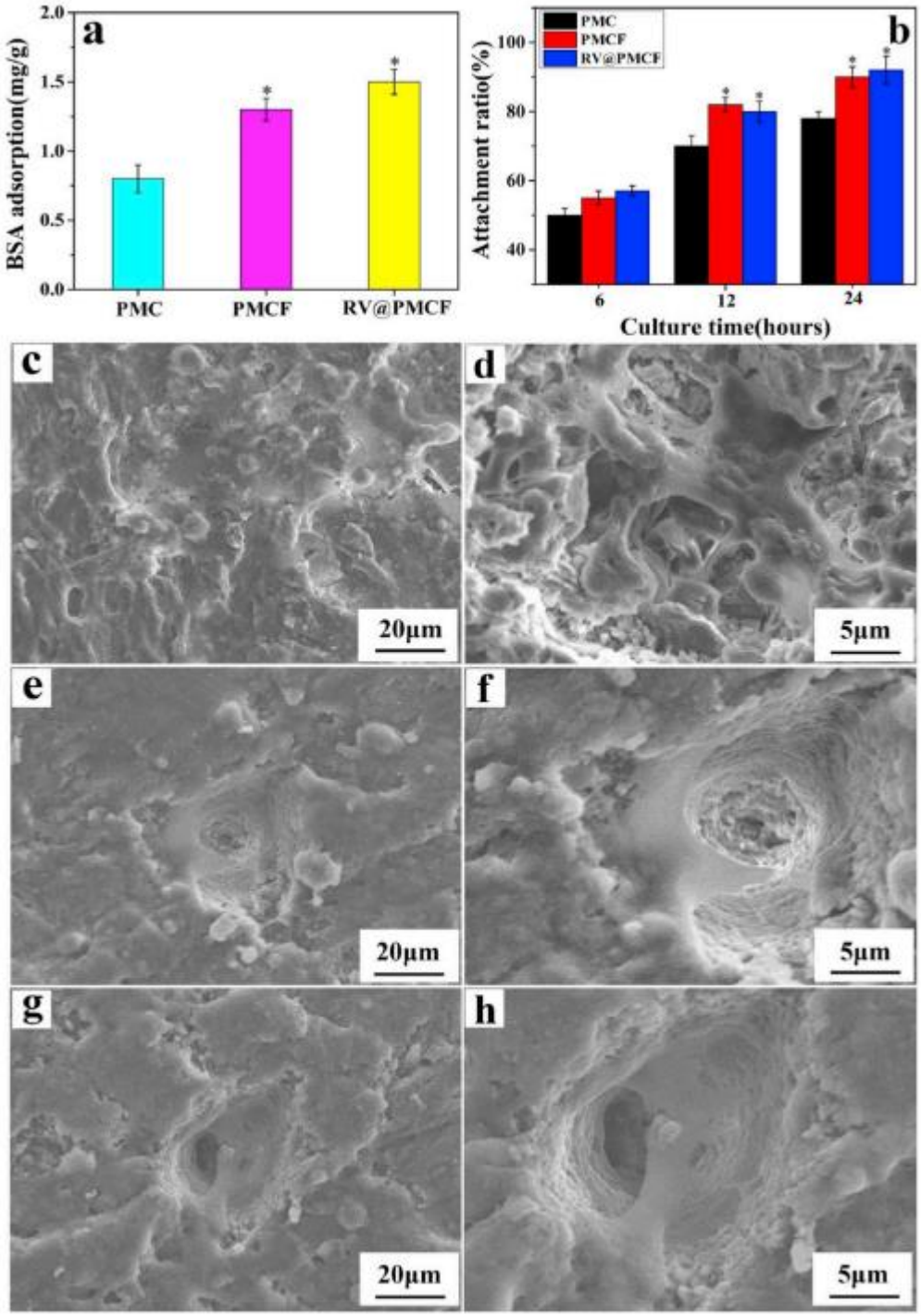

Fig. 6. Adsorption of BSA (a) on the samples, attachment ratio (b) of BMSC on the samples at 6, 12 and 24 h after culturing, and SEM micrographs of BMSC on the surfaces of PMC (c, d), PMCF (e, f) and RV@PMCF (g, h) under different magnification at 24 h after culturing (* represents $p<0.05$, vs PMC).

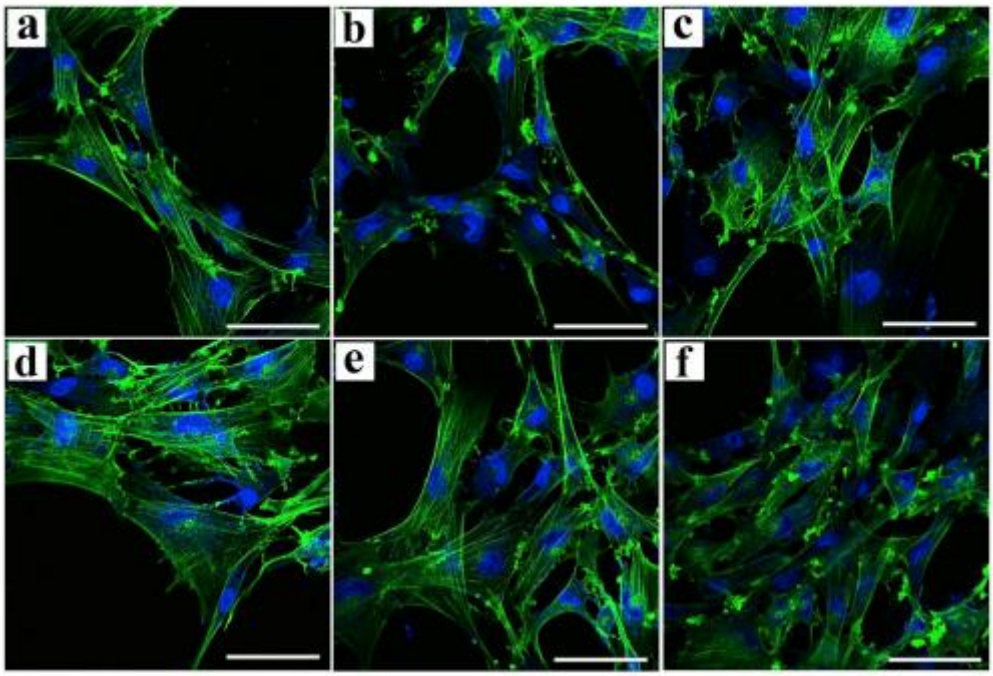

Fig. 7. CLSM images of BMSC on PMC (a, d), PMCF (b, e) and RV@PMCF (c, f) at 3 (a, b, c) and 7 days (d, e, f) after culturing, bar = 20 μm.

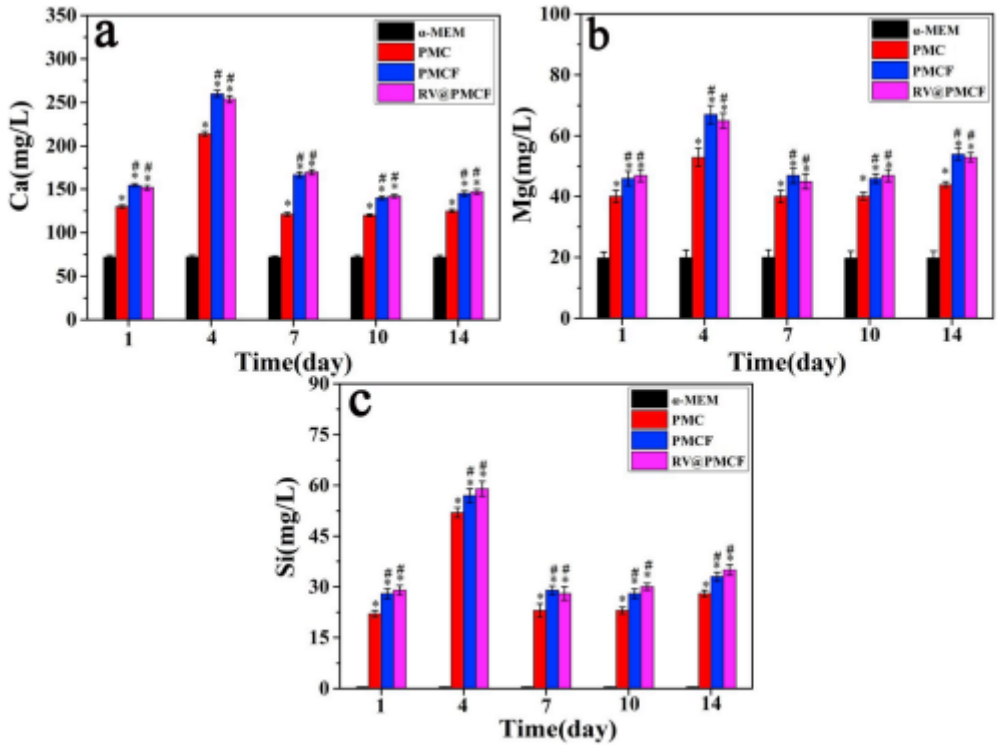

Fig. 8. Change of ions concentrations of Si, Mg and Ca in medium with time after PMC(a), PMCF (b) and RV@PMCF (c) soaked into cell cultured medium for different time (* represents $p < 0.05$,vs a-MEM; # represents $p < 0.05$,vs PMC).

The release of bioactive ions (Si, Mg and Ca) from bioactive materials (bioglass, calcium silicate, etc.) in physiological environment could stimulate the responses of osteoblasts as well as mesenchymal stem cells [**35,36**]. In the present study, the releases of bioactive ions (Si, Mg and Ca) from PMCF and RV@PMCF into the medium were more than PMC. Clearly, the presence of porous surface increased surface area and porosity, and thereby improved these ions release. In addition, no significant difference in ions release between PMCF and RV@PMCF was seen, proving that incorporating of RV did not obviously affect the ions release from RV@PMCF compared with PMCF. Implantable biomaterials for bone regeneration should possess excellent surface bio-properties, which can not only promote cells adhesion and spreading but also stimulate proliferation and osteogenic differentiation as well as new bone regeneration **[37]**. In the present study, compared with PMC, PMCF significantly stimulated cell proliferation due to the release of more bioactive ions. Moreover, compared with PMCF, RV@PMCF remarkably enhanced cell proliferation because of the release of RV. Therefore, the improvement of cell proliferation on RV@PMCF could be ascribed to the combined effect of both hierarchically porous surface (release of more bioactive ions) and slow-release of RV.

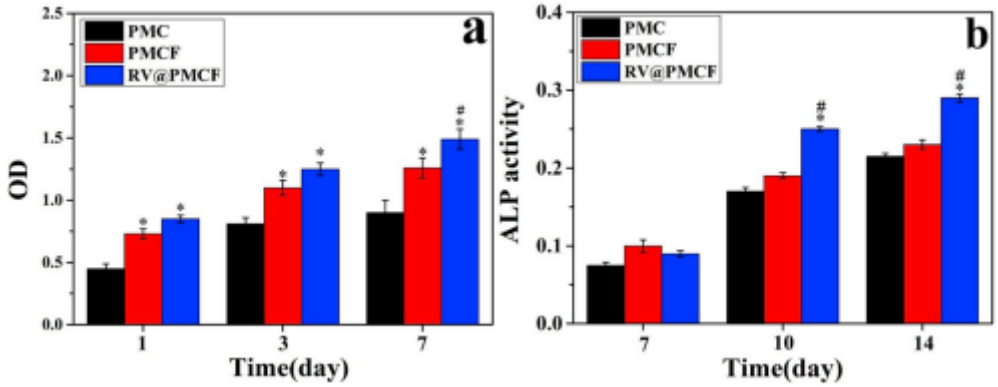

Fig. 9. OD values (a) and ALP activity (b) of BMSC on PMC, PMCF and RV@PMCF at different time after culturing (* represents $p < 0.05$, vs PMC, # represents $p < 0.05$, vs PMCF).

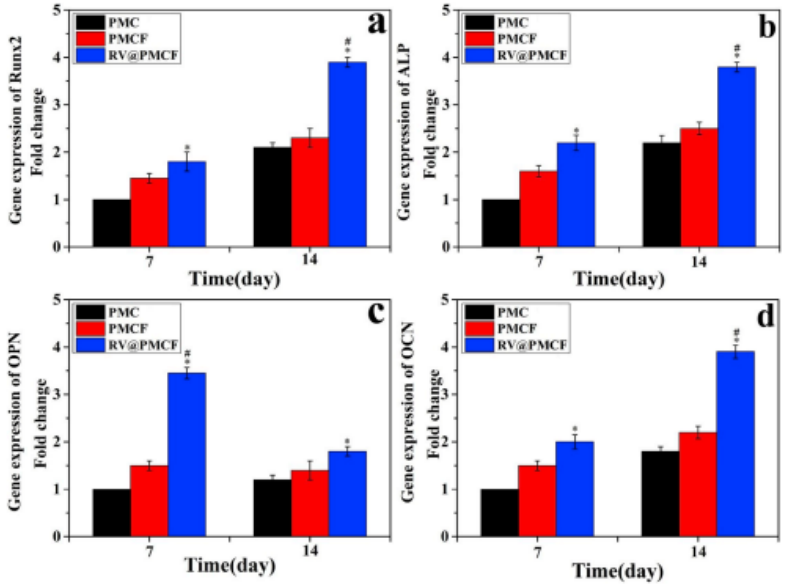

Fig. 10. Expressions of bone related genes (Runx2: a, ALP: b, OPN: c, OCN: d) of BMSC on PMC, PMCF and RV@PMCF at different time after culturing (* representsp < 0.05, vs PMC; # represents $p < 0.05$, vs PMCF).

ALP is an external enzyme of osteoblasts, and the increased expression of ALP activity is a marker of osteogenic differentiation of osteoblasts **[38]**. In the present study, compared with PMC, the ALP activity for PMCF was not remarkably enhanced, revealing that PMCF did not obviously promote the cell differentiation. Moreover, compared to PMCF, the ALP activity for RV@PMCF was significantly improved, suggesting that the release of RV from RV@PMCF promoted the cell differentiation. The Runx2, ALP, OCN and OPN mRNA are the most important genes in osteogenic differentiation of the osteoblasts **[39]**. In the present study, the expressions of these genes of the cells on RV@PMCF were significantly higher than PMCF and PMC, while no significant differences in these genes expression between PMCF and PMC were found. Clearly, the release of RV from RV@PMCF played key roles in promotion of bone related gene expressions. Therefore, compared with PMCF, RV@PMCF significantly enhanced cell differentiation (ALP activity and bone related genes expressions). It could be suggested that the release of RV from RV@PMCF had remarkable influences on osteogenic differentiation of the cells than release of bioactive ions. However, it is hard to separately evaluate each factor. Therefore, the significant enhancements of cells responses would be the cooperative effects of the physical and chemical factors as well as drug of RV.

In conclusion, the hierarchically porous surface and incorporating of RV of RV@PMCF had remarkable influences on the cells behaviours and functions, which were attributed to not only increased surface roughness, protein adsorption and bioactive ions release but also release of RV. Therefore, RV@PMCF displayed outstanding antibacterial properties, cytocompatibility as well as osteogenic activity in vitro. It is expected that after surgical implantation in vivo, the RV@PMCF would form a sustained-release RV at the bone defect, which improves the speed of bone healing.

5. Conclusions

Hierarchically porous surface of PMCF was fabricated by femtosecond laser, and RV was incorporated into the porous surface. Compared to PMC with flat surface, the surface roughness and protein adsorption of both PMCF and RV@PMCF with porous surface were obviously improved thanks to the increased surface area as well as porosity. In addition, the slow-release of RV from RV@PMCF inhibited the growth of both E. coli as well as S. aureus, displaying antibacterial performances. Moreover, compared with PMC, PMCF and RV@PMCF remarkably enhanced adhesion and proliferation of BMSC. Furthermore, compared with PMCF, the release of RV from RV@PMCF significantly promoted proliferation, differentiation and bone related gene expressions of BMSC. In conclusion, PMCF with hierarchically porous surface and incorporation of RV exhibited antibacterial performances and osteogenic activity in vitro. As a drug-loaded implant, RV@PMCF with cytocompatibility would be a great candidate for applications orthopedic fields.

References

[1] Kang KT, Koh YG, Son J, Yeom JS, Park JH, Kim HJ. Biomechanical evaluation of pedicle screw fixation system in spinal adjacent levels using polyetheretherketone, carbon-fiber-reinforced polyetheretherketone, and traditional titanium as rod materials. Compos B Eng 2017;130:248-56.

[2] Ma R, Tang TT. Current strategies to improve the bioactivity of PEEK. Int J Mol Sci 2014;15(4):5426-45.

[3] Kurtz SM, Devine JN. PEEK biomaterials in trauma, orthopedic, and spinal implants. Biomaterials 2007;28(32):4845-69.

[4] Kang KT, Koh YG, Son J, Yeom JS, Park JH, Kim HJ. Highly stable alkaline polymer electrolyte based on a poly(ether ether ketone) backbone. ACS Appl Mater Interfaces 2013;5(24):13405-11.

[5] Zhao Y, Wong HM, Wang WH, Li PH, Xu ZS, Chong EYW, et al. Cytocompatibility, osseointegration, and bioactivity of three-dimensional porous and nanostructured network on polyetheretherketone. Biomaterials 2013;34(37):9264-77.

[6] Liu XL, Han F, Zhao P, Lin C, Wen XJ, Ye XJ. Layer-by-layer self-assembled multilayers on PEEK implants improve osseointegration in an osteoporosis rabbit model. Nanomed-Nanotechnol 2017;13(4):1423-33.

[7] Xu X, Li YL, Wang LX, Li Y, Pan JJ, Fu XM, et al. Triple-functional polyetheretherketone surface with enhanced bacteriostasis and anti-inflammatory and osseointegrative properties for implant application. Biomaterials 2019;212: 98-114.

[8] Tang CY, Tsui CP, Lin W, Uskokovic PS, Wang ZW. Multi-level finite element analysis for progressive damage behavior of HA/PEEK composite porous structure. Compos B Eng 2013;55(9):22-30.

[9] Schambron T, Lowe A, Mcgregor HV. Effects of environmental ageing on the static and cyclic bending properties of braided carbon fibre/PEEK bone plates. Compos B Eng 2008;39(7-8):1216-20.

[10] Lin D, Li Q, Li W, Zhou SW, Swain MV. Design optimization of functionally graded dental implant for bone remodeling. Compos B Eng 2009;40(7):668-75.

[11] Vorobyev AY, Guo CL. Femtosecond laser structuring of titanium implants. Appl Surf Sci 2007;253(17):7272-80.

[12] Vorobyev AY, Guo CL. Direct femtosecond laser surface nano/microstructuring and its applications. Laser Photon Rev 2013;7(3):385-407.

[13] Tiaw KS, Goh SW, Hong M, Wang Z, Lan B, Teoh S. Laser surface modification of poly(e-caprolactone) (PCL) membrane for tissue engineering applications. Biomaterials 2005;26(7):763-9.

[14] Phillips KC, Gandhi HH, Mazur E, Sundaram SK. Ultrafast laser processing of materials: a review. Adv Optic Photon 2015;7(4):684-712.

[15] Karsten K, Raphael AP, Lin L, Grice JE, Soyer HP, Breunig HG, et al. Applications of multiphoton tomographs and femtosecond laser nanoprocessing microscopes in drug delivery research. Adv Drug Deliv Rev 2011;63(4-5):388-404.

[16] Sharahi JY, Azimi T, Shariati A, Safari H, Tehrani MK, Hashemi A. Advanced strategies for combating bacterial biofilms. J Cell Physiol 2019;234(9):14689-708.

[17] Hetrick EM, Schoenfisch MH. Reducing implant-related infections: active release strategies. Chem Soc Rev 2006;35(9):780-9.

[18] Milne JC, Lambert PD, Simon S, Jannin B, Latruffe N. Small molecule activators of SIRT1 as therapeutics for the treatment of type 2 diabetes. Nature 2007;450(7170): 712-6.

[19] Lee IT, Lin CC, Hsu CK, Wu MY, Cho RL, Yang CM. Resveratrol inhibits Staphylococcus aureus -induced TLR2/MyD88/NF-xB-dependent VCAM-1 expression in human lung epithelial cells. Clin Sci 2014;127(5-6):375-90

[20] Li Y, Danmark S, Edlund U, Finne-Wistrand A, He X, Norgard M, et al. Resveratrol-conjugated poly-epsilon-caprolactone facilitates in vitro mineralization and in vivo bone regeneration. Acta Biomater 2011;7(2):751-8.

[21] Martin V, Bettencourt A. Bone regeneration: biomaterials as local delivery systems with improved osteoinductive properties. Mat Sci Eng C-Mater 2017;82:363-71.

[22] Abed E, Couchourel D, Delalandre ADuval N, Pelletier JP, Martel-Pelletier J, et al. Low sirtuin 1 levels in human osteoarthritis subchondral osteoblasts lead to abnormal sclerostin expression which decreases Wnt/p-catenin activity. Bone 2014;59:28-36.

[23] Naruphontjirakul P, Tsigkou O, Li SW, Porter AE, Jones JR. Human mesenchymal stem cells differentiate into an osteogenic lineage in presence of strontium containing bioactive glass nanoparticles. Acta Biomater 2019;90:373-92.

[24] Cai L, Zhang J, Qian J, Li Q, Li H, Yan YG, et al. The effects of surface bioactivity and sustained-release of genistein from a mesoporous magnesium-calcium-silicate/ PK composite stimulating cell responses in vitro, and promoting osteogenesis and enhancing osseointegration in vivo. Biomater Sci 2018;6(4):842-53.

[25] Cai L, Pan YK, Tang SC, Li Q, Tang TT, Zheng K, et al. Macro-mesoporous composites containing PEEK and mesoporous diopside as bone implants: characterization, in vitro mineralization, cytocompatibility, and vascularization potential and osteogenesis in vivo. J Mater Chem B 2017;5(42):8337-52.

[26] Chouirfa H, Bouloussa H, Migonney V, Falentin-Daudre C. Review of titanium surface modification techniques and coatings for antibacterial applications. Acta Biomater 2018;83:37-54.

[27] Choy MT, Tang CY, Chen L, Law WC, Tsui CP, Lu WW. Microwave assisted-in situ synthesis of porous titanium/calcium phosphate composites and their in vitro apatite-forming capability. Compos B Eng 2015;83:50-7.

[28] Asadullah S, Wu H, Mei SQ, Wang DQ, Pan YK, Wang DL, et al. Preparation, characterization, in vitro bioactivity and rBMSCs responses to tantalum pentoxide/ polyimide biocomposites for dental and orthopedic implants. Compos B Eng 2019; 177. UNSP 107433.

[29] Lin LY, Ecke N, Huang MZ, Pei XQ, Schlarb AK. Impact of nanosilica on the friction and wear of a PEEK/CF composite coating manufactured by fused deposition modeling. Compos B Eng 2019;177. UNSP 107428.

[30] Aval NA, Emadi R, Valiani A, Kharaziha M, Karimipour M, Rahbarghazi R. Nanofeatured poly (lactide-co-glycolide)-graphene microribbons as a promising substrate for nerve tissue engineering. Compos B Eng 2019;173. UNSP 106863.

[31] Costerton JW. Bacterial biofilms: a common cause of persistent infections. Science 1999;284(5418):1318-22.

[32] Hwang D, Lim YH. Resveratrol antibacterial activity against Escherichia coli is mediated by Z-ring formation inhibition via suppression of FtsZ expression. Sci Rep 2015;5:10029.

[33] Lord MS, Foss M, Besenbacher F. Influence of nanoscale surface topography on protein adsorption and cellular response. Nano Today 2010;5(1):66-78.

[34] Ross AM, Jiang Z, Bastmeyer M, Lahann J. Physical aspects of cell culture substrates: topography, roughness, and elasticity. Small 2012;8(3):336-55.

[35] Cao LH, Weng WZ, Chen X, Ding YT, Yan YG, Li HH, et al. Development of degradable and bioactive composite as bone implants by incorporation of mesoporous bioglass into poly(l-lactide). Compos B Eng 2015;77:454-61.

[36] Fernandes JS, Gentile P, Pires RA, Reis RL, Hatton PV. Multifunctional bioactive glass and glass-ceramic biomaterials with antibacterial properties for repair and regeneration of bone tissue. Acta Biomater 2017;59:2-11.

[37] Gao C, Peng S, Feng P, Shuai CJ. Bone biomaterials and interactions with stem cells. Bone Res 2017;5:17059.

[38] Zheng D, Neoh KG, Kang ET. Bifunctional coating based on carboxymethyl chitosan with stable conjugated alkaline phosphatase for inhibiting bacterial adhesion and promoting osteogenic differentiation on titanium. Appl Surf Sci 2016; 31:425-34.

[39] Eid AA, Hussein KA, Niu LN, Li GH, Watanabe I, Al-Shabrawey M, et al. Effects of tricalcium silicate cements on osteogenic differentiation of human bone marrow-derived mesenchymal stem cells in vitro. Acta Biomater 2014;10(7):3327-34.